

## In-cell DNP NMR reveals multiple targeting effect of antimicrobial peptide

Frances Separovic<sup>a</sup>, Vinzenz Hofferek<sup>b</sup>, Anthony P. Duff<sup>c</sup>, Malcom J. McConville<sup>b</sup>, Marc-Antoine Sani<sup>a,\*</sup>

<sup>a</sup> School of Chemistry, Bio21 Institute, University of Melbourne, Melbourne, VIC 3010, Australia

<sup>b</sup> Department of Biochemistry and Molecular Biology, Bio21 Institute of Molecular Science and Biotechnology, University of Melbourne, Melbourne, VIC 3010, Australia

<sup>c</sup> National Deuteration Facility, Australian Nuclear Science and Technology Organisation, Kirrawee DC, NSW 2232, Australia

### ARTICLE INFO

#### Keywords:

Antimicrobial peptide  
Bacteria  
In-cell NMR  
Membranes  
DNP  
REDOR

### ABSTRACT

Dynamic nuclear polarization NMR spectroscopy was used to investigate the effect of the antimicrobial peptide (AMP) maculatin 1.1 on *E. coli* cells. The enhanced <sup>15</sup>N NMR signals from nucleic acids, proteins and lipids identified a number of unanticipated physiological responses to peptide stress, revealing that membrane-active AMPs can have a multi-target impact on *E. coli* cells. DNP-enhanced <sup>15</sup>N-observed <sup>31</sup>P-dephased REDOR NMR allowed monitoring how Mac1 induced DNA condensation and prevented intermolecular salt bridges between the main *E. coli* lipid phosphatidylethanolamine (PE) molecules. The latter was supported by similar results obtained using *E. coli* PE lipid systems. Overall, the ability to monitor the action of antimicrobial peptides *in situ* will provide greater insight into their mode of action.

### Introduction

Antibiotic resistance has been observed for several decades, undermining the number of efficacious last resort drugs that are available for treating many infectious diseases (Ventola, 2015). Bacteria have evolved multiple genetic and non-genetic resistance mechanisms against conventional antibiotics that target intracellular cellular processes. In contrast, antimicrobial peptides (AMPs), have a more complex mode of action, and function by targeting bacterial membranes, driven mainly by electrostatic interactions with anionic lipids which are more abundant in prokaryotic than eukaryotic membranes (Sani and Separovic, 2016). This presents less opportunity for bacteria to escape from the effects of AMPs, although some modification of membrane lipid compositions has been observed in response to AMPs (Lee et al., 2021).

AMPs have been investigated for well over five decades, but knowledge of their *in-situ* behaviour is still limited. For instance, while it is possible to obtain the structure of these peptides in model membranes, it has not been possible to obtain details of their mode of action in cells. While it is well established that the majority of AMPs primarily target bacterial membranes, there are indications that their mode of action may be critically dependent on secondary targets or effects (Bahar and Ren, 2013; Huan et al., 2020). Using dynamic nuclear polarization (DNP) enhanced solid-state nuclear magnetic resonance (ss NMR), we report the impact of the AMP, maculatin 1.1 (Mac1) (Le Brun et al.,

2020), on multiple lipid and macromolecular components (i.e., lipids, proteins and nucleic acids) of *Escherichia coli*.

### Material and methods

#### Material

1,2,3-Propanetriol-*d*<sub>8</sub>, deuterated glycerol (glycerol-*d*<sub>8</sub>) and D<sub>2</sub>O were purchased from Sigma-Aldrich (Merck, Sydney, Australia). AMU-Pol was purchased from Cortecnet (Paris, France). Unlabeled maculatin 1.1 (Mac1; GLFGVLAKVAAHVPAIAEHF-NH<sub>2</sub>; M<sub>w</sub> 2145.40) was synthesized manually by solid phase peptide synthesis and purified by HPLC to a purity > 95 % using HCl instead of trifluoroacetic acid salt (Sani et al., 2007). *E. coli* PE lipids were purchased from Avanti Polar Lipids (Alabaster, USA) and used without further purification.

#### Cell growth

*E. coli* BL21 Star<sup>TM</sup> (DE3) cells (Invitrogen, Sydney, Australia) were grown in <sup>13</sup>C, <sup>15</sup>N, <sup>2</sup>H minimal media to exhaustion using the protocol developed by Duff et al. (Duff et al., 2015). The media composition was as reported in Table I of Middelberg et al. (Middelberg et al., 1991) with the following modification: the sole carbon source was 20 g/L glycerol-<sup>13</sup>C<sub>3</sub> (Merck, Sydney, Australia); the sole nitrogen source was 7.8 g/L

\* Corresponding author.

E-mail address: [msani@unimelb.edu.au](mailto:msani@unimelb.edu.au) (M.-A. Sani).

<https://doi.org/10.1016/j.yjsbx.2022.100074>

Received 29 April 2022; Received in revised form 25 July 2022; Accepted 29 August 2022

Available online 13 September 2022

2590-1524/© 2022 The Author(s). Published by Elsevier Inc. This is an open access article under the CC BY-NC-ND license (<http://creativecommons.org/licenses/by-nc-nd/4.0/>).

$^{15}\text{N}$ -ammonium chloride (Cambridge Isotopes, UK); and the water was 99.6 %  $\text{D}_2\text{O}$ . Culturing was performed, from transformation recovery through stepwise flask adaptation to  $\text{D}_2\text{O}$  to bioreactor growth to OD 7.6, at 37 °C. The temperature was then dropped to 14 °C, IPTG added to 1 mM, and culturing continued for another 50 hrs until when the carbon source was exhausted, at OD 13.6, as indicated by a small rise in pH. Cells were harvested by centrifugation, yielding 28.4g wet weight, were frozen in liquid nitrogen, and stored at  $-80$  °C.

3.21 g wet weight of cells were used for this study. The frozen cells were pre-chilled in liquid nitrogen, and placed in the lowest, coldest part of the freeze drier, which was prechilled for main drying (estimated nominal freeze-drying temperature  $-80$  °C). Freeze drying proceeded at a pressure of 0.37 mbar for approximately 90 hrs. The freeze-dried cells weighed 0.645 g (20 % of the wet weight). Dynamic Light Scattering (DLS) was performed on the resuspended cells incubated with and without peptide at 1 mg/ml cell concentration and at 25 °C using a Zetasizer (NanoZS, Malvern, UK). Three biological replicates and three measurements per sample were performed and averaged with particle size and polydispersity values reported in Table S1.

### Lipid extraction

Labeled *E. coli* were fractionated into lipid (apolar) phase, protein, insoluble cell wall (insoluble) phase and polar metabolites (polar) phase using a modified methyl *tert*-butyl ether (MTBE)/ methanol (MeOH) extraction method (Salem et al., 2017). Briefly, 25 mg of a freeze-dried *E. coli* cell pellet was resuspended in 1 mL MTBE/MeOH (3:1, vol/vol) and sonicated for 10 min in an ice-chilled sonicator. 500  $\mu\text{L}$  of water: MeOH (3:1, vol/vol) was added and sample was incubated on a cooled shaker (4 °C, 2000 rpm) for 30 min. Phase separation was introduced by centrifugation (4 °C, 14,000 g, 10 min). The lipid phase was re-extracted twice with 1 mL water:MeOH (3:1, vol/vol). All phases were freeze-dried and stored at  $-20$  °C.

### DNP NMR experiments

Mac1 powder was resuspended in glycerol- $\text{d}_8/\text{D}_2\text{O}/\text{H}_2\text{O}$  (6:3:1, v/v/v) containing 10 mM AMUPol. The solution was used to rehydrate *E. coli* cells, lipid extract or *E. coli* PE lipids at the appropriate ratios for 30 mins at room temperature. The peptide (1 mg) was added to 5 mg of dry cell mass (1 mg  $\sim 2 \times 10^{10}$  cells). This is drastically below MIC but represents  $2.8 \times 10^7$  peptides per cell. The treatment used in this study was solely to assess which cellular targets are affected by the presence of the peptide compared to the control. Two freeze-thaw cycles were performed before packing the sample into a 3.2 mm sapphire rotor.

DNP MAS NMR experiments were conducted on a 9.4 T wide-bore Bruker Avance-III HD DNP NMR Spectrometer (Wissembourg, France) equipped with a 3.2 mm low-temperature triple-resonance MAS probe and a 263.33 GHz gyrotron source. The temperature of all experiments was maintained at 110 K, the spinning frequency was set to 8 kHz.

$^{15}\text{N}$  CPMAS experiments were performed with 100 kHz proton excitation pulse followed by 2 ms Hartmann-Hahn contact with a 30 % RAMP and  $1.3 \times T_{\text{B,on}}$  recycle delay (see Table S1); 32–128 scans and 800 complex points were acquired under 104 kHz SPINAL decoupling. FIDs were zero filled to 4 k points and 100 Hz line broadening was applied.

$^{31}\text{P}$  CPMAS experiments were performed with 100 kHz proton excitation pulse followed by 2.5 ms Hartmann-Hahn contact with a 30 % RAMP and  $1.3 \times T_{\text{B,on}}$  recycle delay (see Table S1); 16–64 scans and 4096 complex points were acquired under 110 kHz SPINAL decoupling. FIDs were zero filled to 16 k points and 80 Hz line broadening was applied. The enhancement  $\epsilon^{\text{DNP}}$  is reported as  $\epsilon_{\text{on}}/\epsilon_{\text{off}}$ .

REDOR experiments were performed under the same CPMAS conditions, using 9  $\mu\text{s}$  and 13.5  $\mu\text{s}$   $\pi$  pulses for  $^{31}\text{P}$  and  $^{15}\text{N}$ , respectively. Several rotor-synchronized dephasing times were acquired with and without the  $^{31}\text{P}$  dephasing pulses. The S and  $S_0$  signal intensities were

estimated from the peak heights. Although the spectra are very convoluted with overlapping signals, the control using pure lipids or nucleic acid confirmed the chemical shifts used for building the dephasing curve.

BS-REDOR fitting program provides the most probable distribution of distance consistent with the REDOR data (Gehman et al., 2007). The fits were optimized using a simulated annealing approach with 100–500 iterations using three stages with a global attenuation temperature of 1.002, Boltzmann factors of 1, 0.5 and 0.0005, initial temperatures of 10, 1 and 0.1, and final temperatures of 0.1, 0.001, 0.00001.

### MD simulations

The CHARMM-GUI membrane builder (Lee et al., 2019) was used to prepare the POPE bilayer system with 48 molecules per leaflet within a rectangular box containing a 12.5 Å layer of water. The simulations were performed using the Charmm36 force field and the minimization, equilibration and production runs were performed with the AMBER CUDA package (Case et al., 2005; Salomon-Ferrer et al., 2013) on a desktop machine fitting a GPU GeForce GTX 1080 titanium and a CPU with 12 cores.

Each system was first minimized for 1000 steps using the steepest descent method followed by 1000 steps of the conjugate gradient method with a 12 Å non-bonded interaction cut-off. The lipids were restrained with a 2.5 kcal.mol $^{-1}$  potential. Then, 1.6 ns equilibration MD simulations were run at 100 K, using decreasing positional restraints to maintain the bilayer structure. All covalent bonds involving hydrogen atoms were constrained using the SHAKE algorithm and the rigid internal geometry for TIP3P water molecules was constrained with the SETTLE algorithm (Miyamoto and Kollman, 1992). The system temperature was maintained at 100 K using a Langevin thermostat (Izaguirre et al., 2001) with a 3 ps $^{-1}$  collision frequency. The system pressure was controlled at 1 bar using a semi-isotropic Monte-Carlo barostat with a xy surface tension. Each restart was performed with a random seed. 100 production runs of 5 ns each were performed.

The MD trajectories were visualized and analyzed using VMD (Humphrey et al., 1996) and the CPPTRAJ (Roe and Cheatham, 2013) program.

### Results

Global scanning of the nitrogen and phosphorus containing cellular components of *E. coli* was achieved by monitoring the nitrogen ( $^{15}\text{N}$ ) signals by cross polarization (CP) magic angle spinning (MAS) NMR of whole bacteria grown in isotopically enriched media ( $^{15}\text{N}$  98 %,  $^{13}\text{C}$  98 % and  $^2\text{H}$  98 % enriched isotopes). Lipids, proteins and nucleic acids display different  $^{15}\text{N}$  chemical shifts that served as an atomic marker for monitoring the action of Mac1 (Fig. 1). DNP-enhanced phosphorous ( $^{31}\text{P}$ ) CPMAS spectra of *E. coli* cells (Fig. S1) displayed little resolution due to high signal overlap of phosphorous containing molecules, such as phospholipids, DNA/RNA or inorganic phosphates. The DNP signal enhancements ( $\epsilon^{\text{DNP}}$ ) and build-up ( $T_{\text{B,on}}$ ) time were more favourable in the presence of Mac1 (Table 1), likely due to uptake by the cell of the radical necessary for DNP signal enhancements (Ghosh et al., 2021) and as previously demonstrated for Mac1 by flow cytometry and fluorescence-activated cell sorting techniques (Sani et al., 2015; Sani et al., 2013). These observations also shows that Mac1 can significantly permeabilize lipid membrane well below its minimum inhibitory concentration (MIC) against *E. coli* ( $\sim 64$   $\mu\text{M}$  at  $5.10^5$  cells). The size measurement of *E. coli* cells resuspended incubated in buffer was of ca. 1.2 nm with low polydispersity of 0.18 (Table S1), which compares well with previous DLS studies (Loske et al., 2014; Vargas et al., 2017). *E. coli* cells incubated in the presence of Mac1 showed a slightly increased diameter of 1.4 nm with a greater polydispersity of 0.4, which within experimental error indicates that the cells are not drastically fragmented, albeit this does not confirm a full cellular integrity.

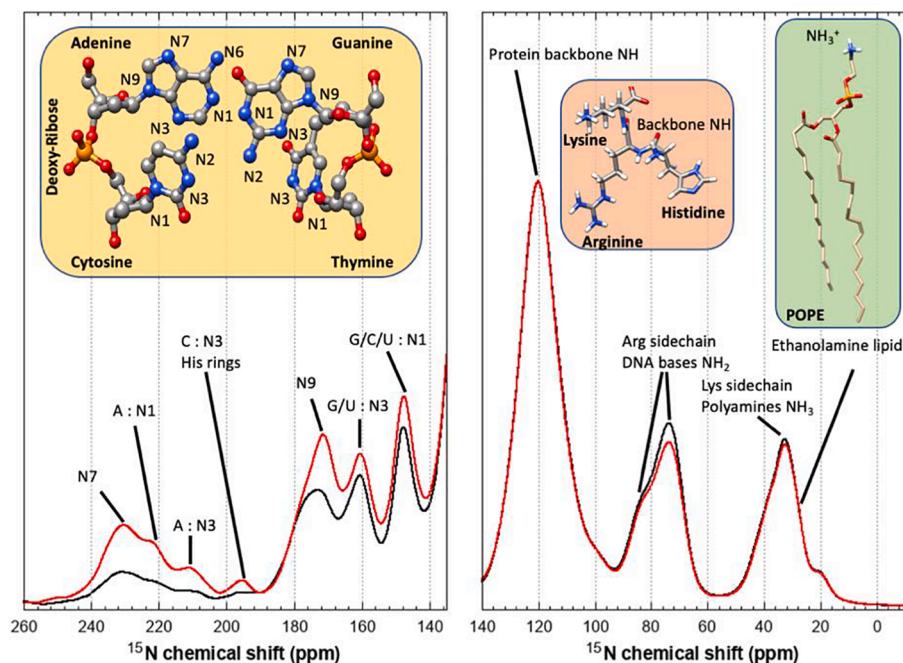


**Fig. 1.** DNP-enhanced  $^{15}\text{N}$  CPMAS spectra of untreated *E. coli* cells (black line) and in the presence of Mac1 at 15:1 w/w ratio (red line). The left panel is scaled 4-fold compared to the right panel to increase visibility. Chemical shift assignments were performed using the BMRB database (<https://bmr.io>). The DNA bases, amino acids with nitrogen containing side-chains and the phospholipid palmitoyl-oleoyl-phosphatidyl-ethanolamine (POPE) structures are displayed in the inserts with nitrogen (blue), oxygen (red), phosphorous (orange), carbon (grey) and hydrogen (white) atoms. (For interpretation of the references to colour in this figure legend, the reader is referred to the web version of this article.)

**Table 1**  
DNP enhancement and build-up time of  $^{31}\text{P}$  CPMAS <sup>a</sup> experiments.

From $^{31}\text{P}$ CPMAS	$T_{B,on}$	$\epsilon^{DNP}$
<i>E. coli</i> cells	9.0 s	79
<i>E. coli</i> cells + Mac1	4.2 s	107
<i>E. coli</i> PE	2.9 s	110
<i>E. coli</i> PE + Mac1	3.2 s	108

<sup>a</sup> performed at 100 K and 8 kHz spinning speed

The DNP NMR experiments were performed at ca. 100 K and the cells are cryoprotected with a glycerol/water mixture, thereby preserving high sample integrity during longer experimental time (Overall et al.,

2019; Sani et al., 2019). As shown in Fig. 1, the resolution of the  $^{15}\text{N}$  signals was not sufficient to observe which moieties were disrupted by Mac1.

This was alleviated by using a novel  $^{15}\text{N}$ - $^{31}\text{P}$  DNP NMR probe configuration (Bruker, Wissembourg, France), which allowed detection of the presence of Mac1 disturbed nitrogen atoms proximal to phosphorous. This is similar to approaches used to detect DNA packaging within bacteriophage T4 (Yu and Schaefer, 2008), protein-RNA complexes (Jehle et al., 2010) or RNA structure (Marchanka et al., 2015). DNP-enhanced REDOR experiments (Gullion, 2006; Schaefer, 2011) were performed, allowing the collection of multiple dephasing times in a shorter timeframe (ca. 30 min per dephasing point). The  $^{15}\text{N}$  observed  $^{31}\text{P}$  dephased REDOR experiments shown in Fig. 2 provide a global scan

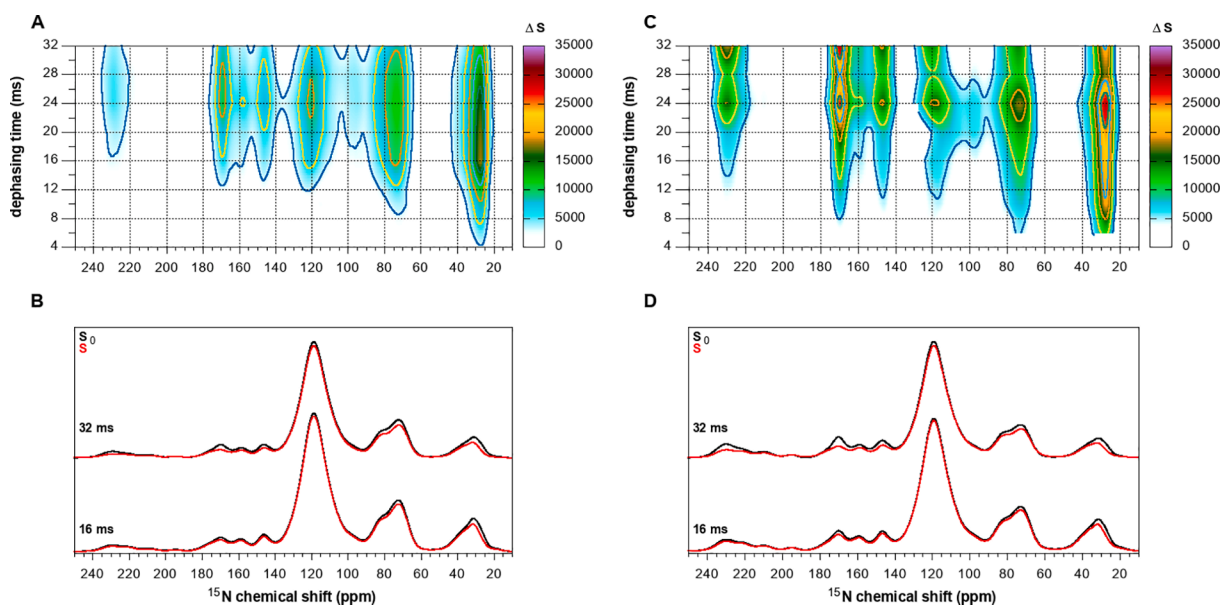


**Fig. 2.** DNP-enhanced  $^{15}\text{N}$  observed  $^{31}\text{P}$  dephased REDOR experiments of untreated *E. coli* (A, B) cells and in the presence of Mac1 at 15:1 w/w ratio (C, D). The  $S_0$  (or  $\Delta S$ ) differences are shown as a 2D map using discrete dephasing time (A, C) while the spectra obtained at 16 ms and 32 ms for both S (black line) and  $S_0$  (red line) are displayed with an offset (B, D). (For interpretation of the references to colour in this figure legend, the reader is referred to the web version of this article.)

of where Mac1-binding impacted *E. coli* main structures. For instance, little effect was observed on the protein NH backbone region while significant signal reductions were observed for NA and lipid regions between 240 and 140 ppm and at ca. 25 ppm, respectively.

Fig. 3 shows the REDOR dephased (*S*) and reference (*S*<sub>0</sub>) spectra at 24 ms dephasing time and dephasing curves for the selected 169 ppm and 25 ppm intensities, corresponding to the nitrogen N9 of nucleic acids and the PE headgroup, respectively. DNP-enhanced <sup>15</sup>N CPMAS spectrum of the single nucleotide adenine was used to support the assignment (Fig. S2). Similarly, lipid extracts from the isotopically enriched *E. coli* cells and liposomes made from *E. coli* PE lipid confirmed that the <sup>15</sup>N chemical shift of the ethanolamine moiety is at ca. 25 ppm (Fig. S3). PE lipids are the most abundant phospholipids (ca. 70 % mol) and the only native lipid in *E. coli* membranes having a nitrogen atom (Lee et al., 2021). The fitting of the *S*/*S*<sub>0</sub> ratio of the REDOR dephasing curves was achieved by using a Boltzmann-statistics (BS) analysis (Gehman et al., 2007). The BS-REDOR analysis does not extract a single distance but instead an ensemble of distances that fit the dephasing curve. Therefore, the span of the ensemble is akin to the standard deviation for each distance population. The ensemble of <sup>31</sup>P-<sup>15</sup>N distances for each region was obtained and confirmed that Mac1-binding leads to tightening the DNA packing (Fig. 3). The analysis showed that the most populated N9 to <sup>31</sup>P distances were shortened by ca. 0.5 Å in the presence of the peptide. However, a significant contribution to the signal is likely due to unperturbed DNA packing. Markedly, the compaction in DNA packing was also observed in our previous study by electron microscopy and <sup>31</sup>P NMR of live *E. coli* incubated with Mac1 (Overall et al., 2019). The analysis of the 25 ppm intensities corresponding mostly to the PE headgroup signal was more intricate. Two populations were obtained with a short distance of ca. 3.7 Å and a broader ensemble at ca. 5.6 Å corresponding to 21 % and 30 % intensity, respectively. The presence of Mac1 did not change significantly the two distances but the

proportion changed to 10 % and 40 %, respectively. It is noteworthy that 50 % of intensity that could not be fit to a discrete distance ensemble arises from the population of <sup>15</sup>N atoms that do not dephase within the dephasing time used (up to 32 ms). It is difficult to accurately extract these longer distances (e.g. > 8 Å is equivalent to a <sup>31</sup>P-<sup>15</sup>N dipolar coupling < 10 Hz) since the REDOR curve is dominated by the stronger couplings. Moreover, the short distances are likely to provide the most important information regarding the molecular packing, and disruption upon incubation with the AMP.

Comparable results were produced using multilamellar membranes made from *E. coli* PE lipids (Fig. 4). Interestingly, the dephasing curves obtained in the lipid only system with or without Mac1 showed almost full dephasing within 32 ms while only ca. 50 % dephasing was reached in *E. coli* cells. This may indicate that *in situ*, molecular packing is mediating NMR results. Nevertheless, the similar shift in population towards the more distant <sup>31</sup>P-<sup>15</sup>N population was reproduced. Molecular dynamics (MD) was used to investigate the PE membrane packing. The simulation showed that the PE amine group has the tendency to form intermolecular bridges, with adjacent phosphate groups having shorter distance (around 3.7 Å) compared to the intramolecular nitrogen to phosphorous distance (broader distribution around 4.3 Å). The NMR data showing that Mac1 disrupted these stabilising interactions suggest that the antimicrobial peptide, below MIC, is weakening the lipid bilayer packing.

## Conclusion

This in-cell NMR study revealed that membrane-active AMPs can have a multi-target impact on *E. coli* cells. At sub-MIC concentration, the antimicrobial peptide Mac1 induced both NA condensation and prevented intermolecular salt bridge in lipid membrane (Fig. 5).

This first report of an *in situ* investigation of Mac1 in *E. coli* using

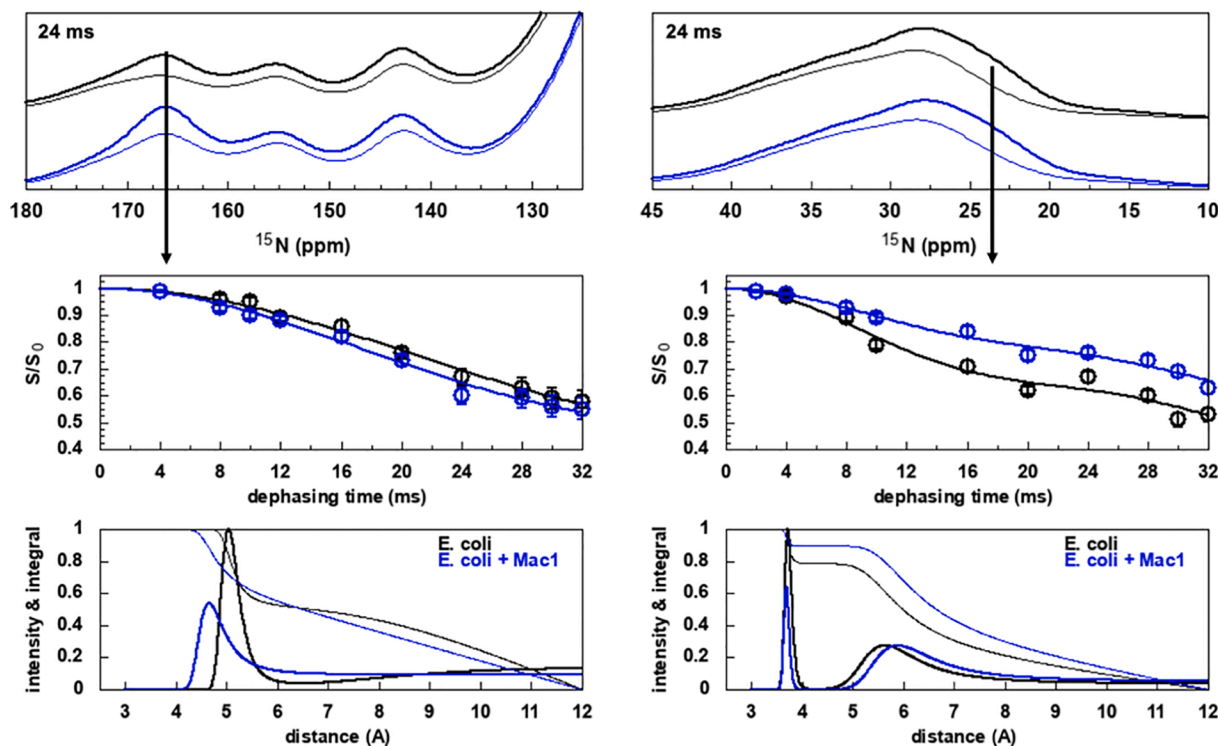
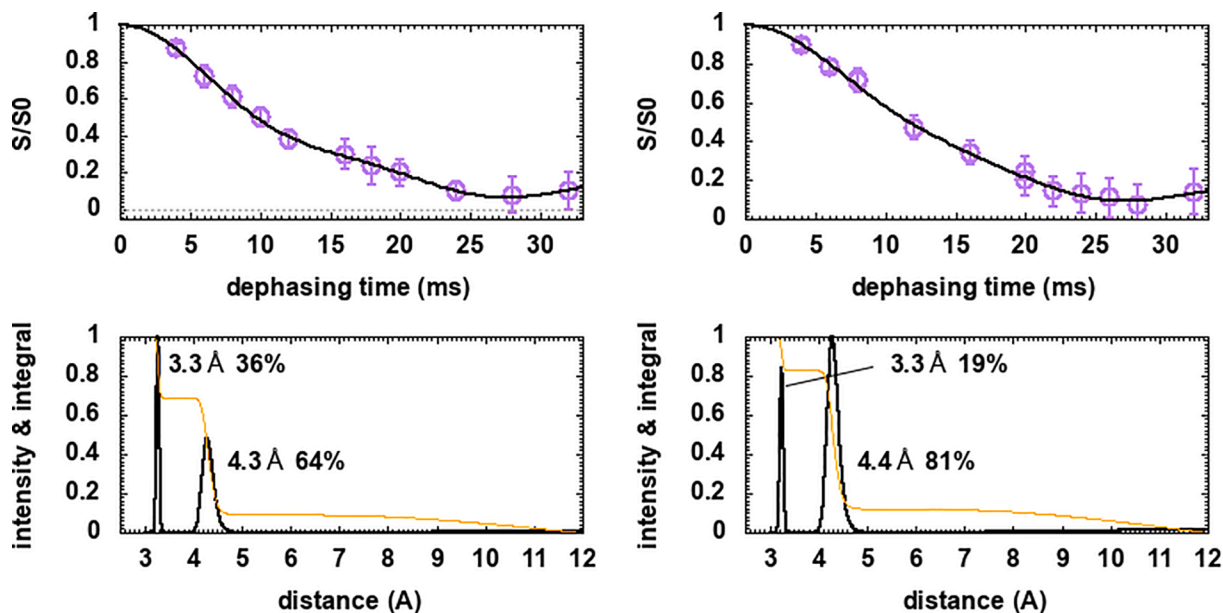
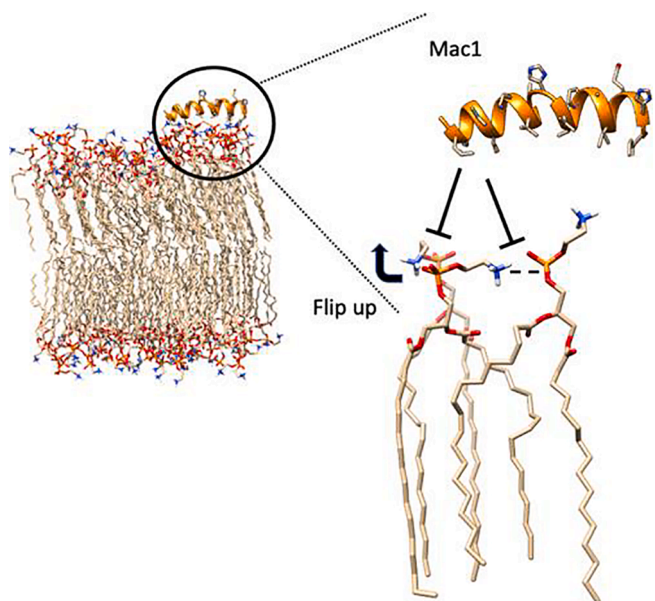


Fig. 3. (Top panel) REDOR spectra for (left) the nitrogen N9 at 165 ppm, and (right) the lipid region of *E. coli* cells (black lines) and in the presence of Mac1 (blue lines) at 15:1 w/w ratio with (dark lines) the reference spectra (*S*<sub>0</sub>) and (light lines) the dephased spectra (*S*) shown. (Middle panel) REDOR dephasing curves for (left) the nitrogen N9 at 165 ppm, and (right) the lipid region of *E. coli* cells (black lines) and in the presence of Mac1 (blue lines). (Bottom panel) Maximum entropy reconstruction of the distance ensembles fitting the REDOR dephasing curves. The distances (solid line intensities) and population (light lines) integrals are plotted on the same scale. (For interpretation of the references to colour in this figure legend, the reader is referred to the web version of this article.)



**Fig. 4.** (top panels) REDOR dephasing curves for (left) untreated *E. coli* PE and (right) in the presence of Mac1 at 19:1 mol/mol. (Bottom panel) Maximum entropy reconstruction of the distance ensembles fitting the REDOR dephasing curves. The distances (solid black line intensities) and population (light orange lines) integrals are plotted on the same scale. (For interpretation of the references to colour in this figure legend, the reader is referred to the web version of this article.)



**Fig. 5.** Representation of the impact of Mac1 onto POPE lipid bilayers. Mac1 breaches the intermolecular salt bridge between adjacent PE headgroups by preventing the amine group from bending inward, thereby reducing the packing in lipid membrane.

DNP-enhanced  $^{15}\text{N}$  detected NMR opens new avenues for detecting the global impact of antimicrobial peptides on intact cellular systems. This approach could be combined with  $^{13}\text{C}$  observed  $^{31}\text{P}$  dephased TEDOR/REDOR experiments to gain an extra level of high-resolution structural details. Similarly, specific labelling schemes could be applied with  $^{15}\text{N}$ -labelled cells and  $^{13}\text{C}$ -labelled peptides to gain further resolution and, together with DNP-enhanced experiments, provide the signal boost necessary for observing dilute spin systems *in-situ*.

#### CRedit authorship contribution statement

**Frances Separovic:** Conceptualization, Project administration,

Funding acquisition. **Vinzenz Hofferek:** Methodology, Investigation, Validation. **Anthony P. Duff:** Methodology, Investigation, Resources, Validation. **Malcom J. McConville:** Resources. **Marc-Antoine Sani:** Conceptualization, Methodology, Resources, Validation, Formal analysis, Project administration.

#### Declaration of Competing Interest

The authors declare that they have no known competing financial interests or personal relationships that could have appeared to influence the work reported in this paper.

#### Acknowledgements

This work was supported by the Australian Research Council [LE160100120, DP160100959, DP190101506 and DP210101792]. Access to NMR spectrometers was provided by the Bio21 Institute at the University of Melbourne. The National Deuteration Facility is partly supported by the National Collaborative Research Infrastructure Strategy – an initiative of the Australian Government.

#### Appendix A. Supplementary data

Supplementary data to this article can be found online at <https://doi.org/10.1016/j.jysbx.2022.100074>.

#### References

- Bahar, A., Ren, D., 2013. Antimicrobial Peptides. *Pharmaceuticals (Basel)* 6 (12), 1543–1575.
- Case, D.A., Cheatham 3rd, T.E., Darden, T., Gohlke, H., Luo, R., Merz Jr., K.M., Onufriev, A., Simmerling, C., Wang, B., Woods, R.J., 2005. The Amber biomolecular simulation programs. *J. Comput. Chem.* 26, 1668–1688.
- Duff, A.P., Wilde, K.L., Rekas, A., Lake, V., Holden, P.J., 2015. Robust high-yield methodologies for  $(2)\text{H}$  and  $(2)\text{H}/(15)\text{N}/(13)\text{C}$  labeling of proteins for structural investigations using neutron scattering and NMR. *Methods Enzymol.* 565, 3–25.
- Gelman, J.D., Separovic, F., Lu, K., Mehta, A.K., 2007. Boltzmann statistics rotational-echo double-resonance analysis. *J. Phys. Chem. B* 111 (27), 7802–7811.
- Ghosh, R., Xiao, Y., Kragelj, J., Frederick, K.K., 2021. In-Cell Sensitivity-Enhanced NMR of Intact Living Mammalian Cells. *bioRxiv*, 2021.2005.2028.446194.
- Gullion, T., 2006. Rotational-Echo, Double-Resonance NMR. In: Webb, G.A. (Ed.), *Modern Magnetic Resonance*. Springer, Netherlands, Dordrecht, pp. 713–718.

- Huan, Y., Kong, Q., Mou, H., Yi, H., 2020. Antimicrobial Peptides: Classification, Design, Application and Research Progress in Multiple Fields. *Front. Microbiol.* 11.
- Humphrey, W., Dalke, A., Schulten, K., 1996. VMD: Visual molecular dynamics. *J. Mol. Graph.* 14, 33–38.
- Izaguirre, J.A., Catarello, D.P., Wozniak, J.M., Skeel, R.D., 2001. Langevin stabilization of molecular dynamics. *J. Chem. Phys.* 114, 2090–2098.
- Jehle, S., Falb, M., Kirkpatrick, J.P., Oschkinat, H., van Rossum, B.J., Althoff, G., Carlomagno, T., 2010. Intermolecular protein-RNA interactions revealed by 2D 31P–15N magic angle spinning solid-state NMR spectroscopy. *J. Am. Chem. Soc.* 132, 3842–3846.
- Le Brun, A.P., Zhu, S., Sani, M.-A., Separovic, F., 2020. The Location of the Antimicrobial Peptide Maculatin 1.1 in Model Bacterial Membranes. *Front. Chem.* 8.
- Lee, T.-H., Hofferek, V., Sani, M.-A., Separovic, F., Reid, G.E., Aguilar, M.-I., 2021. The impact of antibacterial peptides on bacterial lipid membranes depends on stage of growth. *Faraday Discuss.*
- Lee, J., Patel, D.S., Stähle, J., Park, S.J., Kern, N.R., Kim, S., Lee, J., Cheng, X., Valvano, M.A., Holst, O., Knirel, Y.A., Qi, Y., Jo, S., Klauda, J.B., Widmalm, G., Im, W., 2019. CHARMM-GUI Membrane Builder for Complex Biological Membrane Simulations with Glycolipids and Lipoglycans. *J. Chem. Theory Comput.* 15, 775–786.
- Loske, A.M., Tello, E.M., Vargas, S., Rodriguez, R., 2014. Escherichia coli viability determination using dynamic light scattering: a comparison with standard methods. *Arch. Microbiol.* 196, 557–563.
- Marchanka, A., Simon, B., Althoff-Ospelt, G., Carlomagno, T., 2015. RNA structure determination by solid-state NMR spectroscopy. *Nat. Commun.* 6, 7024.
- Middelberg, A.P.J., O'Neill, B.K.L., Bogle, I.D., Snoswell, M.A., 1991. A novel technique for the measurement of disruption in high-pressure homogenization: Studies on E. coli containing recombinant inclusion bodies. *Biotechnol. Bioeng.* 38, 363–370.
- Miyamoto, S., Kollman, P.A., 1992. Settle: An analytical version of the SHAKE and RATTLE algorithm for rigid water models. *J. Comput. Chem.* 13, 952–962.
- Overall, S.A., Zhu, S., Hanssen, E., Separovic, F., Sani, M.-A., 2019. In Situ Monitoring of Bacteria under Antimicrobial Stress Using 31P Solid-State NMR. *Int. J. Mol. Sci.* 20.
- Roe, D.R., Cheatham, T.E., 2013. PTRAJ and CPPTRAJ: Software for Processing and Analysis of Molecular Dynamics Trajectory Data. *J. Chem. Theory Comput.* 9, 3084–3095.
- Salem, M., Bernach, M., Bajdzienko, K., Giavalisco, P., 2017. A Simple Fractionated Extraction Method for the Comprehensive Analysis of Metabolites, Lipids, and Proteins from a Single Sample. *J. Vis. Exp.*
- Salomon-Ferrer, R., Götz, A.W., Poole, D., Le Grand, S., Walker, R.C., 2013. Routine Microsecond Molecular Dynamics Simulations with AMBER on GPUs. 2. Explicit Solvent Particle Mesh Ewald. *J. Chem. Theory Comput.* 9, 3878–3888.
- Sani, M.A., Separovic, F., 2016. How Membrane-Active Peptides Get into Lipid Membranes. *Acc. Chem. Res.* 49, 1130–1138.
- Sani, M.A., Loudet, C., Gröbner, G., Dufourc, E.J., 2007. Pro-apoptotic bax-alpha1 synthesis and evidence for beta-sheet to alpha-helix conformational change as triggered by negatively charged lipid membranes. *J. Pept. Sci.* 13, 100–106.
- Sani, M.A., Whitwell, T.C., Gehman, J.D., Robins-Browne, R.M., Pantarat, N., Attard, T. J., Reynolds, E.C., O'Brien-Simpson, N.M., Separovic, F., 2013. Maculatin 1.1 Disrupts Staphylococcus aureus Lipid Membranes via a Pore Mechanism. *Antimicrob. Agents Chemother.* 57, 3593–3600.
- Sani, M.A., Henriques, S.T., Weber, D., Separovic, F., 2015. Bacteria May Cope Differently from Similar Membrane Damage Caused by the Australian Tree Frog Antimicrobial Peptide Maculatin 1.1. *J. Biol. Chem.* 290, 19853–19862.
- Sani, M.A., Zhu, S., Hofferek, V., Separovic, F., 2019. Nitroxide spin-labeled peptides for DNP-NMR in-cell studies. *FASEB J.* 33, 11021–11027.
- Schaefer, J., 2011. "Development of REDOR rotational-echo double-resonance NMR" by Terry Gullion and Jacob Schaefer [J. Magn. Reson. 81 (1989) 196–200]. *J. Magn. Reson.* 213, 421–422.
- Vargas, S., Millan-Chiu, B.E., Arvizu-Medrano, S.M., Loske, A.M., Rodriguez, R., 2017. Dynamic light scattering: A fast and reliable method to analyze bacterial growth during the lag phase. *J. Microbiol. Methods* 137, 34–39.
- Ventola, C.L., 2015. The antibiotic resistance crisis: part 1: causes and threats. *P T* 40, 277–283.
- Yu, T.Y., Schaefer, J., 2008. REDOR NMR characterization of DNA packaging in bacteriophage T4. *J. Mol. Biol.* 382, 1031–1042.